CrystEngComm

Accepted Manuscript

ROYAL SOCIETY OF CHEMISTRY

www.rsc.org/crystengcomm

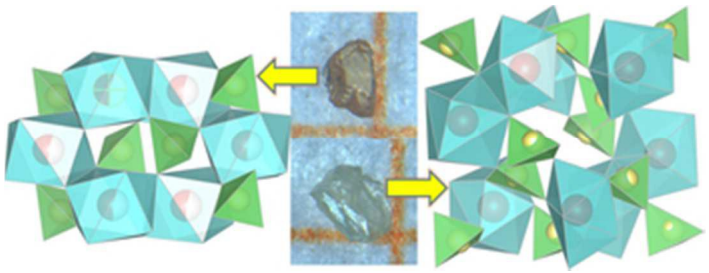

29x11mm (300 x 300 DPI)

Journal Name

ARTICLE

Effect of high bismuth deficiency on structure and oxide ion conductivity of $Bi_{0.55}MoO_4$ single crystal

Received 00th January 20xx,
Accepted 00th January 20xx

DOI: 10.1039/x0xx00000x

www.rsc.org/

Yang Zhang,[ab] Hengjiang Cong,[a] Nianjing Ji,[a] Jian Liu,[a] Xiulan Duan,[a] Jing Li,[a] Wenwu Cao,[b] Jiyang Wang,[a] and Huaidong Jiang*[a]

We report, for the first time,the ionic conductivity properties of two polymorphic structures of bismuth molybdates: $Bi_{0.55}MoO_4$ and $Bi_2(MoO_4)_3$. $Bi_{0.55}MoO_4$ single crystal was first synthesized,existing a surprisingly high bismuth deficiency as compared to the known stoichiometric phase $Bi_2(MoO_4)_3$. It is expected to have a good oxide ion conduction due to the presence of Bi deficiency and oxygen vacancies. $Bi_{0.55}MoO_4$ crystallizes in the tetragonal system, space group $I4_1/a$ with a=b=5.239(2), c=11.567(5) Å, and Z=4. While $Bi_2(MoO_4)_3$ crystallizes in monoclinic space group $P2_1/n$, with unit cell parameters a=7.71500(10), b=11.5101(2), c=11.1237(2) Å, β = 103.3640(10)°, and Z=4. Taking an advantage over many other ionic conductors, the crystals do not undergo any clear structural phase transition below their melting points. The oxide ion conductivities of $Bi_{0.55}MoO_4$ and $Bi_2(MoO_4)_3$ were measured to be 6.5×10^{-5} S/cm and 1.1×10^{-6} S/cm at a temperature of 400 °C, respectively.

Introduction

Oxide ion conductors are an important class of functional materials with wide applications in oxygen sensors, oxygen pumps, and oxygen-permeable membrane catalysts, as well as electrolytes in solid oxide fuel cells (SOFCs).[1-5] Over the past few decades, many efforts have been made to develop new oxide ion conductive materials which possess high oxide ion mobilities at low operating temperature.[1,6,7] However, the compounds which have high ionic conduction by oxygen ions are rather rare, mainly due to the fact that oxygen ions species have a large ionic radius in comparison with the other atoms in the structure.[8]

Currently existing oxide ion conductors are essentially confined to a small group with fluorite structures, the most important examples being ZrO_2-,[9,10] Bi_2O_3-[11,12] and CeO_2-related materials[13]. Another commonly used type of oxide ion conductors has perovskite structure, such as $LaGaO_3$,[14-16] $NdAlO_3$,[17,18]and $Ba_2In_2O_5$[19,20]. However, the idealized fluorite and perovskite structures do not contain oxygen vacancies, and the structures are extremely versatile.[21] By doping +2 or +3 ions into the lattice, oxygen vacancies are produced in order to balance the charge. Oxide ion conduction then proceeds through oxygen 'jumps' via these vacancy defects.[22,23] A novel oxide ion conductor $La_2Mo_2O_9$ was discovered by P. Lacorre and F. Goutenoire in 2000.[6,24] Its conductivity is about 6×10^{-2} S·cm^{-1} at 800 °C because of a structural transition, which is comparable to that of stabilized zirconia.

Bismuth oxides exhibit both a high oxide ion conductivity and electrocatalytic activity for the interconversion of molecular O_2 and ionic O^{2-} at low temperature (300-500 °C), and thus have an important potential for oxygen generating.[7] In the long-term exploration, many bismuth molybdates have been found, among which the highest conductivities belong to $Bi_{26}Mo_{10}O_{69}$[21] and $Bi_{37.5}Mo_{7.5}O_{78.75}$[22].

Oxide ion conductors are usually served as a form of polycrystalline thin film for most applications. However, pores, grain boundaries and intergranular phases in the polycrystalline materials are inevitable obstacles to investigate intrinsic bulk conductivity of the oxide ions.[23] Therefore, single crystals are necessary to investigate their intrinsic properties. In this paper, millimeter-sized $Bi_{0.55}MoO_4$ and $Bi_2(MoO_4)_3$ single crystals were grown using a spontaneous nucleation method. We report the crystal, electronicstructures and possible mechanism for the oxide ion migration for $Bi_{0.55}MoO_4$ and $Bi_2(MoO_4)_3$. Although $Bi_2(MoO_4)_3$ was reported by A.F. Van den Elzen et.al in 1973, the oxygen ion conductivity property remains unknown up to now. $Bi_{0.55}MoO_4$ single crystal was synthesized for the first time, which is a non-stoichiometric compound with bismuth deficiency. Oxygen vacancies are created to maintain an overall electrical neutrality for charge compensation purposes. The high concentration of oxygen vacancy provides a channel for oxygen ions migration. Therefore, the new crystal $Bi_{0.55}MoO_4$ is expected to have excellent oxygen ionic conductivity properties.

Experimental Procedure

[a]State Key Laboratory of Crystal Materials, Shandong University, 27 Shandanan Road, Jinan, 250100, China.
[b]Department of Mathematics and Materials Research Institute, Pennsylvania State University, University Park, Pennsylvania 16802, USA
E-mail: hdjiang@sdu.edu.cn

† Footnotes relating to the title and/or authors should appear here.
Electronic Supplementary Information (ESI) available: [details of any supplementary information available should be included here]. See DOI: 10.1039/x0xx00000x

Synthesis

Bi_2O_3 (Aldrich, 99+%), H_3BO_3 (Alfa Aesar, 99.99%), MoO_3 (Alfa Aesar, 99.99%), and Li_2CO_3 (Aldrich, 99+%) were used as received. Single crystal $Bi_{0.55}MoO_4$ was grown with a ratio of Bi_2O_3: H_3BO_3: MoO_3: Li_2CO_3 = 1: 2: 5: 1. Mixtures of the four starting materials were placed in a Φ35×35 mm^3 platinum crucible. The crucible was gradually heated to 650 °C in air, held for 24 h, and then cooled slowly to 500 °C at a rate of 2.5 °C /h, followed by rapid cooling to room temperature. H_3BO_3 and Li_2CO_3 play a role of flux, and the B^{5+} and Li^+ ions do not enter into the lattice based on measurement. In order to study the relationship between the two similar compounds, $Bi_2(MoO_4)_3$ was grown in a stoichiometric mixture of Bi_2O_3 and MoO_3.

Characterisation

In order to confirm and identify the phase purity of $Bi_{0.55}MoO_4$ and $Bi_2(MoO_4)_3$, X-ray powder diffraction analysis was performed in a 2θ range from 10° to 80° on an automated Bruker D8 diffractometer equipped with a diffracted beam monochromatic set for Cu K_α (λ=1.5418 Å) radiation and a nickel filter at room temperature. Elemental analysis was carried out on a Hitachi S4100T scanning electron microscope with energy-dispersive X-ray microanalysis (Oxford INCA Energy).

The structures of $Bi_{0.55}MoO_4$ and $Bi_2(MoO_4)_3$ crystals were determined by single crystal X-ray diffraction on a Bruker SMART APEX-II diffractometer using monochromatic Mo-K_α Radiation at 296(2) K integrated with the SAINT program. A brown crystal (0.11×0.08×0.06 mm^3) of $Bi_{0.55}MoO_4$ and a light yellow crystal (0.09×0.08×0.06 mm^3) of $Bi_2(MoO_4)_3$ were used for single crystal data collection. A wavelength of 0.71073 Å was used to minimize absorption. All calculations were performed with programs from the SHELXTL crystallographic software package. All of the atoms were refined with anisotropic thermal parameters and converged for I>2σ. Crystallographic data for the reported materials are shown in Table 1.

DTA was conducted by NETZSCH STA 409C (Germany) from 20 to 1100 °C in N_2. The DTA measurement was performed inside an evacuated silica ampule. The samples were heated to 1000 °C with a rate of 10 °C /min.XPS was performed in order to confirm the existence of oxygen vacancy in $Bi_{0.55}MoO_4$. XPS spectra of both $Bi_{0.55}MoO_4$ and $Bi_2(MoO_4)_3$ were obtained with a Thermofisher ESCALAB 250 X-ray photoelectron spectrometer using an Al Ka (1486.6 eV) source in ultrahigh vacuum (10^{-7} Pa). Powder samples were mounted on a piece of double-sided Cu tape and attached to the XPS sample holder. The binding energy was calibrated by using C1s peak (284.8 ev) as a reference. UV-vis diffuse reflectance spectra were measured with a U-4100 Spectrophotometer (Solid) in the wavelength from 300 nm to 2500 nm.

$Bi_{0.55}MoO_4$ and $Bi_2(MoO_4)_3$were first grinded in an agate mortar, and the powder were pressed to dense pellets with 15 mm diameter and 1 mm thickness using a spark plasma sintering system (580 °C, 70 GPa). The pellets were coated with thin platinum films on both flat faces as electrodes using magnetron sputtering. Then the edges were lightly grinded to remove the platinum pasted on the edge. The prepared pellets were used for the direct-current (DC) electrical conductivity measurements. The current-voltage (I-V) characteristics were measured with a Keithley 2410 sourcemeter by two-probe method. The data were measured in the temperature range of 160–420 °C in ambient air. In the heating runs, the increment of temperature was 10 °C. Before each measurement, the sample was kept at the indicated temperature for 5 min.The ionic conductivities were then calculated with the formula σ=L/(R*S), where R is the resistance from the measurements, and L and S are the thickness and surface area of the samples.

Computational Descriptions

The theoretical calculations were performed using the plane-wave pseudopotential method based on the density functional theory (DFT) with the generalized gradient approximation (GGA) in the scheme of Perdew–Burke–Ernzerhof.[25] The geometry optimization task was taken by the crystallographic data obtained from the X-ray diffraction. The ultrasoft pseudo-potentials were applied for the interactions between electrons and ionic cores. The energy band structure was calculated along the high-symmetry directions in the Brillouin zone. The following orbital electrons were treated as valence electrons: O-$2s^2 2p^4$, Bi-$6s^2 6p^3$, Mo-$5s^1 4p^6 4d^5$. For the sampling of the Brillouin zone, the electronic structures and optical properties used 6×6×1 k-point grids generated according to the Monkhorst-Pack scheme.[26]

Results and Discussion

The XRD patterns of $Bi_{0.55}MoO_4$ and $Bi_2(MoO_4)_3$ are shown in Fig. 1.The experimental XRD profile of $Bi_{0.55}MoO_4$ is well-indexed with the calculated result from Material Studio 6.0 using CASTEP module. The experimental XRD pattern of $Bi_2(MoO_4)_3$ is also consistent with pdf#21-0103 of $Bi_2(MoO_4)_3$. The XRD data shows that both $Bi_{0.55}MoO_4$ and $Bi_2(MoO_4)_3$ are well crystallized and the phase purity is high.

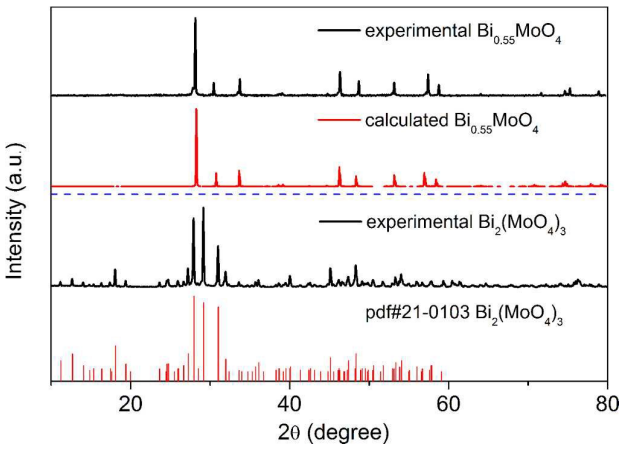

Fig. 1 XRD patterns of experimental $Bi_{0.55}MoO_4$, calculated $Bi_{0.55}MoO_4$, experimental $Bi_2(MoO_4)_3$, and pdf#21-0103 for $Bi_2(MoO_4)_3$.

To determine the radio of Bi^{3+} and Mo^{6+} ions in $Bi_{0.55}MoO_4$ and $Bi_2(MoO_4)_3$, Energy Dispersive Spectroscopy (EDS) measurements were performed. The results show that the radios of Bi^{3+} and Mo^{6+} are about 0.56 in $Bi_{0.55}MoO_4$ and 0.68 in $Bi_2(MoO_4)_3$ (see Fig. S1 in the Supporting Information), which are in good agreement with the radios in their chemical formula.

Scheelites exist in a wide range of compositions and have a rather open crystal structure, which can be simply thought of as a modification of the fluorite structure with an ordered arrangement of the two cations.[27] $Bi_{0.55}MoO_4$ belongs to the scheelite structure of $CaWO_4$, isomorphic with $Eu_2(WO_4)_3$ and $Nd_2(MoO_4)_3$. For $Eu_2(WO_4)_3$, the crystal structure can be viewed as a stacking up of Ca^{2+} and WO_4^{2-} ions in scheelite, where every three Ca^{2+} ions have been replaced by two Eu^{3+} ions and a vacancy. These vacancies are ordered in planes parallel to the *a* and *b* axes.[28] Since the non-stoichiometric properties of $Bi_{0.55}MoO_4$, it could have a much larger number of vacancies than $Eu_2(WO_4)_3$. At room temperature, $Bi_{0.55}MoO_4$ crystallizes in tetragonal space group with unit cell parameters a=b=5.239(2), c=11.567(5) Å, and Z=4. Two BiO_8dodecahedra are linked to MoO_4tetrahedraby sharing a common oxygen atom (see Fig. 2a). The BiO_8dodecahedra in $Bi_{0.55}MoO_4$ possess D_{2d} symmetry, with the two independent Bi-O(A) and Bi-O(B) distances, at 2.469(3) Å and 2.487(3) Å, differing by less than one pooled standard deviation. MoO_4 tetrahedra are regular tetrahedron with a Mo-O bond length of 1.776(3) Å. Deficiency in the A cation site leads to ordering of the structures and oxygen vacancies, and may further lead to an increase in conductivity, which has been confirmed in the following sections.

The crystal structure of $Bi_2(MoO_4)_3$ was first reported by A.F. Van den Elzen et.al,[28] and then redetermined by F. Theobald.[29] The structure of $Bi_2(MoO_4)_3$ is also consisted of two BiO_8dodecahedraand one MoO_4 tetrahedra by sharing a common oxygen atom(Fig. 2b). However, the BiO_8 dodecahedra and MoO_4 tetrahedra in $Bi_2(MoO_4)_3$ are more distorted than those in $Bi_{0.55}MoO_4$. There are 13 independent Bi-O distances varying from 2.145 Å to 2.751 Å. The Mo-O distance varies between 1.707Å and 2.293Å, and the average of the Mo-O distance among three different MoO_4 tetrahedra varies between 1.870Å and 1.897A˚. The refine data for $Bi_{0.55}MoO_4$ and $Bi_2(MoO_4)_3$ are shown in Table 1. Interatomic distances, the atomic coordinates and their equivalent isotropic thermal parameters for $Bi_{0.55}MoO_4$ and $Bi_2(MoO_4)_3$ are summarized in Tables S1, S2, S3 and S4 in the Supporting Information.

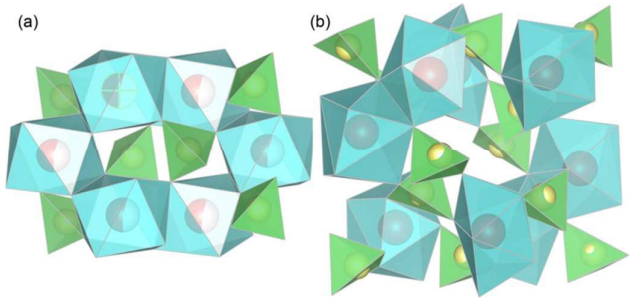

Fig. 2 Crystal structures of (a) $Bi_{0.55}MoO_4$ and (b) $Bi_2(MoO_4)_3$.

Table 1 Crystal data at 296 K and structure refinement for $Bi_{0.55}MoO_4$ and $Bi_2(MoO_4)_3$.

	$Bi_{0.55}MoO_4$	$Bi_2(MoO_4)_3$
formula weight	274.88	897.78
temperature (K)	296(2)	296(2)
wavelength (Å)	0.71073	0.71073
crystal system	tetragonal	monoclinic
space group	I 4_1/a	P2_1/n
unit cell dimensions (Å)	a=b=5.239(2), c=11.567(5)	a=7.71500(10), b=11.5101(2), c=11.1237(2)
volume (Å^3)	317.5(3)	961.04(3)
Z	4	4
density (g/cm^3) calcd	5.750	6.205
absorption coefficient (mm^{-1})	34.291	40.369
F(000)	479	1552
crystal size (mm)	0.11×0.08×0.06	0.09×0.08×0.06
Θ range for data collection (°)	4.270-27.833	2.58-27.00
limiting indices	-6 ≤ h ≤ 6, -6 ≤ k ≤ 6, -14 ≤ l ≤ 15	-9 ≤ h ≤ 9, -14 ≤ h ≤ 14, -14 ≤ h ≤ 14,
reflections collected	1861	18848
Independent reflections	192 (R_{int}=0.0491)	2092 (R_{int}=0.0534)
refinement method	full-matrix least-squares on F^2	full-matrix least-squares on F2
data/restraints/parameters	192/0/16	2092/0/155
goodness-of-fit on F^2	1.102	1.149
final R indices [I>2ó(I)]	R_1=0.0180, wR_2=0.0474	R_1=0.0237, wR_2=0.0587
R indices (all data)	R_1= 0.0195, wR_2=0.0486	R_1=0.0247, wR_2=0.0595
extinction coefficient	0.055(3)	0.00596(17)
largest diff. peak and hole (eÅ^{-3})	0.786 and -0.468	2.841 and -1.012

The DTA curves of $Bi_{0.55}MoO_4$ and $Bi_2(MoO_4)_3$ were measured to study the phase transition and melting point, and the results are shown in Fig. 3. From the figure, one can see that there is only one endothermic peak corresponding to the melting point for the both samples, and no phase transition is observed upon heating the samples in evacuated and sealed silica ampules up to 1000 °C. The melting points of $Bi_{0.55}MoO_4$ and $Bi_2(MoO_4)_3$ are 661 °C and 663 °C, respectively. $Bi_{0.55}MoO_4$ can be considered as an bismuth deficient compound rooted from $Bi_2(MoO_4)_3$. The existence of oxygen vacancies has little influence to the melting point. Moreover, no extra impurity peaks were found in the DTA curves, which also confirmed the single phases of the crystals.

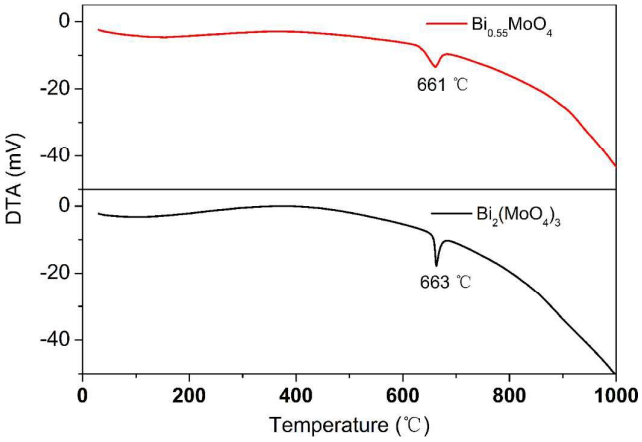

Fig. 3 The DTA curve of $Bi_{0.55}MoO_4$ and $Bi_2(MoO_4)_3$.

X-ray photoelectron spectroscopy analysis was carried out to confirm the existence of oxygen vacancy in $Bi_{0.55}MoO_4$, and a comparison with $Bi_2(MoO_4)_3$was also made and shown in Fig. 4. The asymmetric O 1s peak in $Bi_{0.55}MoO_4$ was fitted by two nearly Gaussian components, low-binding-energy component centered at 530. 9 eV (Oa) and high-binding-energy component 532.8 eV (Ob), respectively, as shown in the upper half of Fig.4. The black line is the experimental result, and the green line is the fitted result. The asymmetry of the main peak is due to the existence of a large number of oxygen vacancies,[30,31] and the fitted peak Ob represents the oxygen vacancies. Changes in the intensities of Oa and Ob may be correlated with the variations in the concentration of the oxygen vacancies (V_O).[32] However, the O 1s peak in $Bi_2(MoO_4)_3$ is nearly symmetrical (see the lower part of Fig. 4), which indicates that few oxygen vacancies exist in the crystal. This result is consistent with the experimental and calculated optical absorption below. The XPS spectra of Bi 4f, Mo 3d and survey are shown in Figures S2, S3 and S4 in the Supporting Information.

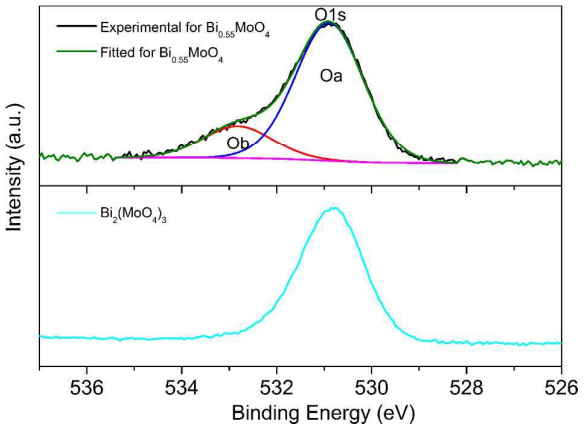

Fig. 4 Oxygen 1s XPS spectra of $Bi_{0.55}MoO_4$ and $Bi_2(MoO_4)_3$.

To better understand the influence of oxygen vacancy on structure, bonding and optical absorption, first principles calculations were performed on the structures of $Bi_{0.55}MoO_4$ and $Bi_2(MoO_4)_3$. The calculated band structures for $Bi_{0.55}MoO_4$ and $Bi_2(MoO_4)_3$along high symmetry directions in the Brillouin zone are plotted with the energy zero corresponding to the valence-band top (Fig. S5 in the Supporting Information). The band gaps of $Bi_{0.55}MoO_4$ and $Bi_2(MoO_4)_3$ are 2.45 eV and 3.11 eV, respectively. Although the chemical compositions of the two compounds are very similar, the energy bands show large differences. The band of $Bi_{0.55}MoO_4$ has a larger fluctuation, and electron localization decreases. It is easier for the electron in the valence band to hop into the conduction band. While the band of $Bi_2(MoO_4)_3$ is relatively flat, which indicates that the chemical properties may be more stable.

The calculated TDOS and PDOS for $Bi_{0.55}MoO_4$ and $Bi_2(MoO_4)_3$ are shown in Fig. 5. The states in conduction band of $Bi_{0.55}MoO_4$ are broader than those of $Bi_2(MoO_4)_3$, which corresponds to the energy band structures. The broad states in conduction indicate that $Bi_{0.55}MoO_4$ has a stronger metallicity and may be a promising candidate for oxygen ions conduction. The states at much lower energy do not participate in bonding, so they are not shown here. The valence bands are mainly composed of O 2s and Mo 4d, and the conduction bands are chiefly consisted of Bi 6p and Mo 4d.

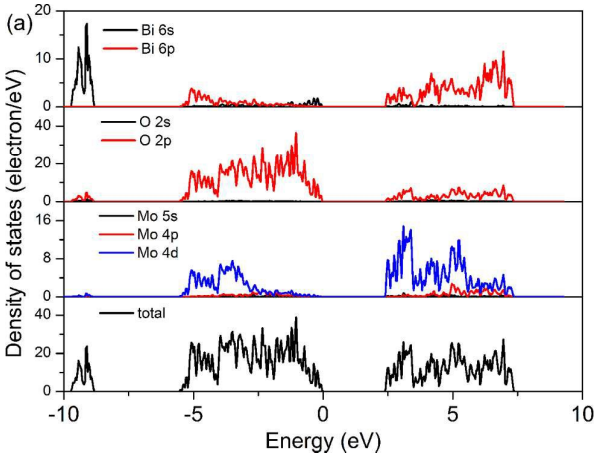

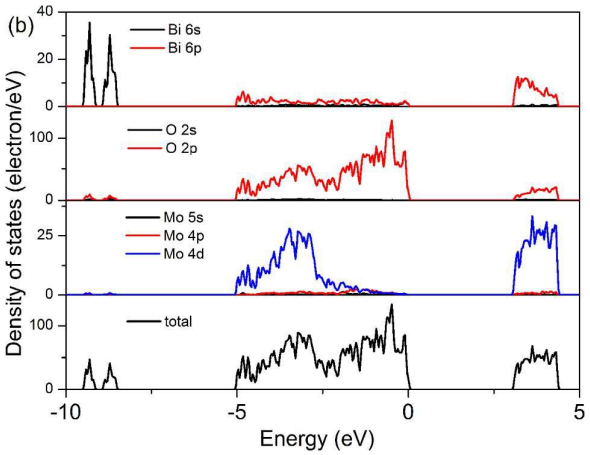

Fig. 5 The total density of states (TDOS) and the partial density of states (PDOS) of different atoms in (a) $Bi_{0.55}MoO_4$ and (b) $Bi_2(MoO_4)_3$.

UV-vis-NIR diffuse reflectance spectra of $Bi_{0.55}MoO_4$ and $Bi_2(MoO_4)_3$ crystals are shown in Fig. 6. We can observe that the absorption of $Bi_{0.55}MoO_4$in the visible region is obviously higher than $Bi_2(MoO_4)_3$ from the inset in Fig. 7. Due to the existence of oxygen vacancies, the color of $Bi_{0.55}MoO_4$ is brown and leads to a higher absorption. Both of them have a cutoff edge about 358 nm. In order to confirm the experimental optical absorption results in theory, we calculate the optical absorption using DFT method and the result is shown in Fig. 7. $Bi_{0.55}MoO_4$ has a higher absorption all over the wavelength, which further confirms the experimental results. The Bi deficiency and oxygen vacancies in $Bi_{0.55}MoO_4$ give rise to a higher optical absorption than $Bi_2(MoO_4)_3$.

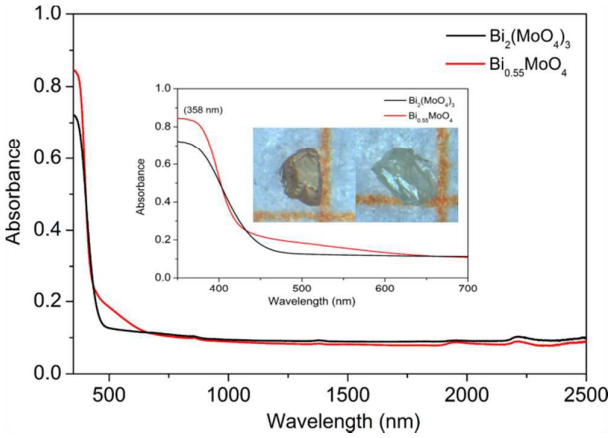

Fig. 6 UV-vis-NIR diffuse reflectance spectra of $Bi_{0.55}MoO_4$ and $Bi_2(MoO_4)_3$. An inset shows the variation of absorption in the visible region. Crystal photographs of $Bi_{0.55}MoO_4$ (brown one on the left) and $Bi_2(MoO_4)_3$ (light yellow one on the right) are shown in the inset.

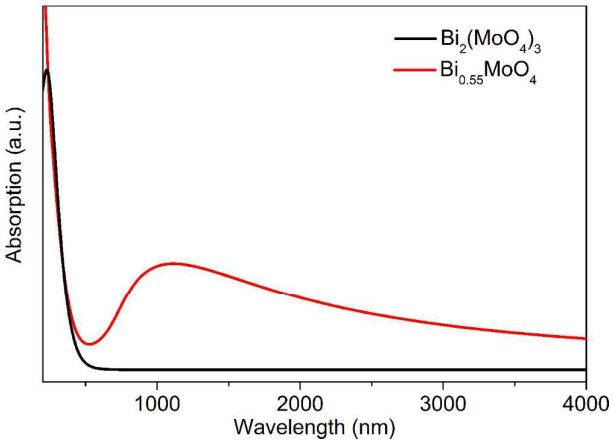

Fig. 7 The calculated absorption spectra of $Bi_{0.55}MoO_4$ and $Bi_2(MoO_4)_3$.

Fig. 8 shows the conductivities of the $Bi_{0.55}MoO_4$ and $Bi_2(MoO_4)_3$ measured at 160−420 °C in air. The oxide ion conductivities of $Bi_{0.55}MoO_4$ and $Bi_2(MoO_4)_3$ show big differences and reach 6.5×10^{-5} S/cm and 1.1×10^{-6} S/cm at a temperature of about 400 °C, respectively. In addition, the conductivities of both materials have an increasing trend above the measured temperature.

For lanthanum-strontium gallates and aluminates, A-site deficiency will increase the ionic conductivity.[32,33] The ionic electronic conductivity was found to increase when cation vacancies are created in the A sublattice of perovskite-type $Sr_{1-y}Fe_{0.8}Ti_{0.2}O_{3-\delta}$ (y=0-0.06).[34] Such improvement of conductivity was attributed in part to an increased oxygen-vacancy concentration from the A-site deficiency. In our experiments, the Bi deficiency and oxygen vacancies in $Bi_{0.55}MoO_4$ also cause a much higher conductivity than that of $Bi_2(MoO_4)_3$, and hence $Bi_{0.55}MoO_4$ is expected to be a potential candidate for oxide-ion conductor.

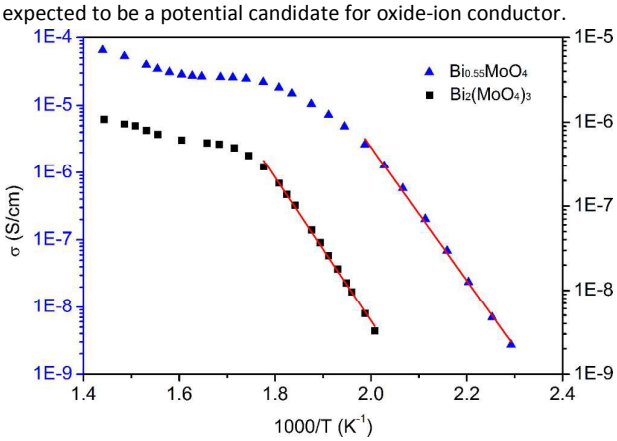

Fig. 8 Variation of conductivity versus temperature for $Bi_{0.55}MoO_4$ and $Bi_2(MoO_4)_3$.

Conclusion

In conclusion, a new bismuth deficientmolybdate$Bi_{0.55}MoO_4$ and its stoichiometric phase $Bi_2(MoO_4)_3$ were synthesized using spontaneous nucleation method in air. Compositions of single-phase structures and the ratios of Bi and Mo ions in

both compounds were confirmed using PXRD and EDS. Structural analysis shows a significant difference between these two molybdate materials. Based on DTA analysis in both materials, no phase transitions were observed below their melting points. The existence of a large number of oxygen vacancies in $Bi_{0.55}MoO_4$ was confirmed by both XPS and first-principle calculation. These high concentrations of oxygen vacancies intrinsically embedded in the crystal lattice enhance the oxygen ion diffusion. Therefore, $Bi_{0.55}MoO_4$presents a larger conductivity than $Bi_2(MoO_4)_3$ due to the bismuth deficiency and large number of oxygen vacancies, and could be a good potential candidate for oxygen ion conductors.

Acknowledgements

We thank Prof. Minglei Zhao and Dan Yu for the measurement of conductivity. This work was supported by the National Natural Science Foundation of China (31430031, U1332118).

Notes and references

1 J. Boivin, G. Mairesse, *Chem.Mater.*, 1998, **10**, 2870-2888.
2 P. Lacorre, F. Goutenoire, O. Bohnke, R. Retoux, Y. Laligant, *Nature*, 2000, **404**, 856-858.
3 J.B. Goodenough, Nature, 2000, **404**, 821-823.
4 M.-H.l.n. Chambrier, A. Le Bail, F. Giovannelli, A. Redjaimia, P. Florian, D. Massiot, E. Suard, F. Goutenoire, *Inorg.Chem.*, 2013, **53**, 147-159.
5 F. Henn, R. Buchanan, N. Jiang, D. Stevenson, *Appl. Phys. A*, 1995, **60**, 515-519.
6 S. Ikeda, O. Sakurai, K. Uematsu, N. Mizutani, M. Kato, *J. Mater. Sci.*, 1985, **20**, 4593-4600.
7 R. Punn, A.M. Feteira, D.C. Sinclair, C. Greaves, *J. Am. Chem. Soc.*, 2006, **128**, 15386-15387.
8 T. Takahashi, T. Esaka, H. Iwahara, *J. Appl. Electrochem.*, 1977, **7**, 303-308.
9 H. Inaba, H. Tagawa, *Solid State Ionics*, 1996, **83**, 1-16.
10 T. Ishihara, H. Matsuda, Y. Takita, *J. Am. Chem. Soc.*, 1994, **116**, 3801-3803.
11 T. Ishihara, M. Honda, T. Shibayama, H. Minami, H. Nishiguchi, Y. Takita, *J. Electrochem.Soc.*, 1998, **145**, 3177-3183.
12 T. Ishihara, H. Matsuda, Y. Takita, *Solid State Ionics*, 1995, **79**, 147-151.
13 T. Ishihara, H. Matsuda, Y. Takita, *J. Electrochem.Soc.*, 1994, **141**, 3444-3449.
14 T. Ishihara, H. Matsuda, Y. Mizuhara, Y. Takita, *Solid State Ionics*, 1994, **70**, 234-238.
15 P. Berastegui, S. Hull, F. Garcıa-Garcıa, S.-G. Eriksson, *J. Solid State Chem.*, 2002, **164**, 119-130.
16 S. Stølen, C.E. Mohn, P. Ravindran, N.L. Allan, *J. Phys. Chem. B*, 2005, **109**, 12362-12365.
17 K.R. Kendall, C. Navas, J.K. Thomas, H.-C.z. Loye, *Solid State Ionics*, 1995, **82**, 215-223.
18 E. Kendrick, J. Kendrick, K.S. Knight, M.S. Islam, P.R. Slater, *Nat.Mater.*, 2007, **6**, 871-875.
19 X. Kuang, M.A. Green, H. Niu, P. Zajdel, C. Dickinson, J.B. Claridge, L. Jantsky, M.J. Rosseinsky, *Nat.Mater.*, 2008, **7**, 498-504.
20 F. Goutenoire, O. Isnard, R. Retoux, P. Lacorre, *Chem.Mater.*, 2000, **12**, 2575-2580.
21 G. Mairesse, F. Abraham, G. Nowogrocki, *J. Solid State Chem.*, 1996, **122**, 394-406.
22 X. Kuang, Y. Li, C.D. Ling, R.L. Withers, I.R. Evans, *Chem. Mater.*, 2010, **22**, 4484-4494.
23 M. Higuchi, Y. Masubuchi, S. Nakayama, S. Kikkawa, K. Kodaira, *Solid State Ionics*, 2004, **174**, 73-80.
24 J.P. Perdew, K. Burke, M. Ernzerhof, *Phys.Rew.Lett.*, 1996, **77**, 3865.
25 H.J. Monkhorst, J.D. Pack, *Phys. Rev. B*, 1976, **13**, 5188.
26 L. Hoffart, U. Heider, R. Huggins, W. Witschel, R. Jooss, A. Lentz, *Ionics*, 1996, **2**, 34-38.
27 A. Van den Elzen, G. Rieck, *Acta Crystallogr. B: Struct. Crystallogr. and Cryst. Chem.*, 1973, **29**, 2433-2436.
28 F. Theobald, A. Laarif, A. Hewat, *Mater.Rev.Bull.*, 1985, **20**, 653-665.
29 P. Mohanty, N.C. Mishra, R.J. Choudhary, A. Banerjee, T. Shripathi, N.P. Lalla, S. Annapoorni, C. Rath, *J. Phys. D: Appl. Phys.*, 2012, **45**, 325301.
30 H. Ren, G. Xiang, G. Gu, X. Zhang, W. Wang, P. Zhang, B. Wang, X. Cao, *J. Nanomater.*, 2012, **2012**, 1-5.
31 M. Chen, X. Wang, Y. Yu, Z. Pei, X. Bai, C. Sun, R. Huang, L. Wen, *Appl. Surf. Sci.*, 2000, **158**, 134-140.
32 J.W. Stevenson, T.R. Armstrong, L.R. Pederson, J. Li, C. Lewinsohn, S. Baskaran, *Solid State Ionics*, 1998, **113**, 571-583.
33 T.L. Nguyen, M. Dokiya, S. Wang, H. Tagawa, T. Hashimoto, *Solid State Ionics*, 2000, **130**, 229-241.
34 A. Kovalevsky, V. Kharton, V. Tikhonovich, E. Naumovich, A. Tonoyan, O. Reut, L. Boginsky, *Mat. Sci. Eng. B*, 1998, **52**, 105-116.